JOURNAL OF GEOPHYSICAL RESEARCH, VOL. 87, NO. B7, PAGES 5327–5338, JULY 10, 1982

Controlled Electromagnetic Sources for Measuring Electrical Conductivity Beneath the Oceans 1. Forward Problem and Model Study

ALAN D. CHAVE

Institute of Geophysics and Planetary Physics, Scripps Institution of Oceanography, University of California, San Diego La Jolla, California 92093

CHARLES S. COX

Ocean Research Division, Scripps Institution of Oceanography, University of California, San Diego La Jolla, California 92093

Exact closed-form expressions for the electromagnetic induction fields produced by vertical and horizontal current sources in the conducting ocean overlying a one-dimensional earth are derived from the Maxwell equations. Numerical methods for the evaluation of the solutions are given, including correction for the finite size of real sources. Simple models of the electrical conductivity structure of the ocean crust and lithosphere are deduced from geologic, petrologic, and laboratory data, and their electromagnetic response is modeled. Horizontal electric dipole sources produce much larger field amplitudes than their vertical counterparts for a given frequency and range, and the horizontal electric field offers superior received signal performance. Reflections of electromagnetic waves from the sea surface and thermocline must be considered for low enough frequencies or long ranges. Estimates of the ambient noise level from natural electromagnetic sources in the frequency range 0.01—10 Hz are presented. The ability of controlled sources to determine features of the conductivity of the ocean crust and upper mantle, especially low conductivity zones, is demonstrated. If the mantle conductivity is low enough, horizontal ranges of 50 km and conductivity estimates to over 20 km depth can be achieved.

INTRODUCTION

Over the past two decades, natural electromagnetic fields at the floor of the deep ocean have been measured and used to infer the electrical conductivity of the upper mantle by the magnetotelluric method [*Cox et al.*, 1970; *Filloux*, 1980, 1981; *Law and Greenhouse*, 1981; *Chave et al.*, 1981]. All of these studies indicate rising conductivity at depths of 60—200 km, but the data are unable to resolve either the conductivity of the crust and lithosphere or the thickness of the high-conductivity region underlying the lithosphere. This is due in large part to the band limited nature of the natural electromagnetic spectrum beneath the ocean. At frequencies above a few cph the ionospheric signals at the seafloor are attenuated by the conducting seawater and masked by various forms of oceanic background noise (e.g., induction from turbulent water motions, surface, and internal waves). The magnetotelluric method is a valuable tool for probing deep earth structure, but it is not likely that improvements in data quality will allow it to be used for lithospheric studies.

The oceanic lithosphere is a region of changing temperature and composition whose detailed structure is governed by the dynamic processes of plate accretion. Electrical conductivity is sensitive mainly to temperature, composition, and the degree of partial melting [cf. *Shankland*, 1975]; thus indirect measurements of it would constrain earth models and complement the data available from other geophysical disciplines. The existence of a low-conductivity zone in the lithosphere is suggested by laboratory measurements of minerals. Such a region would exert a profound influence on the interpretation of both the motional induction fields caused by large scale oceanic flow and magnetotelluric experiments in the ocean-continent transition zone [*Cox*, 1980, 1981; *Ranganyaki and Madden*, 1980].

Cox et al. [1978] measured the natural background noise in the seafloor electric field at frequencies around 1 Hz and obtained a level near 1 pV/m. This very low value suggests that the weak electromagnetic fields that propagate in the underlying sediments, crust, and lithosphere from a sea bottom mounted artificial source are measurable at significant source-receiver separations. There are four fundamental electromagnetic source types: vertical and horizontal electric dipoles (VED and HED), consisting of an insulated, current-carrying wire with bared ends, and vertical and horizontal magnetic dipoles (VMD and HMD), consisting of closed loops of insulated, current-carrying wire. VED and HED oceanic methods have been proposed [*Edwards et al.*, 1981; *Cox et al.*, 1981], and an experiment on the East Pacific Rise yielded measurements of the horizontal electric field from an HED source at a range of 19 km [*Young and Cox*, 1981].

It is the purpose of this paper to develop the necessary theory to calculate the electromagnetic induction fields from controlled sources in the ocean and apply it to models of the oceanic crust and mantle. Equations for induction by horizontal and vertical current elements are

Paper number 2B0583.
0148-0227/82/002B-0583$05.00

derived from the Maxwell equations, and exact solutions suitable for numerical evaluation are obtained. Any of the four artificial source types can be constructed from these expressions by suitable integrations. Electromagnetic waves generated at the ocean-crust interface damp out rapidly with range, in contrast to the terrestrial situation. Combined with the low ambient noise level, this yields much greater sensitivity of electromagnetic methods in the ocean compared to land. We illustrate this by modeling some simple oceanic crustal conductivity structures.

The emphasis in this paper is on the forward geophysical problem and the ability to detect changes of conductivity at depth in the earth. In a subsequent paper, we will examine the inverse problem for an artificial source and investigate the separate question of resolution capability.

GOVERNING EQUATIONS

The fundamental equations for electromagnetic induction are the Maxwell equations with the displacement current neglected

$$\nabla \cdot \vec{B} = 0 \tag{1}$$

$$\nabla \times \vec{E} + i\omega\vec{B} = 0 \tag{2}$$

$$\nabla \times \vec{B} - \mu\sigma\vec{E} = \mu\vec{J}^0 \tag{3}$$

where $\vec{E}$ is the electric field, $\vec{B}$ is the magnetic induction, μ is the magnetic permeability, σ is the electrical conductivity, a single Fourier component proportional to $e^{i\omega t}$ is considered, and the source current $\vec{J}^0$ is treated explicitly. Note that $\vec{E}$ is the induced electric field; the total electric field is given by $\vec{E} + \vec{J}^0/\sigma$. Equations (1)—(3) can be solved numerically for arbitrary μ and σ, but closed forms exist when only one-dimensional variations of these parameters are allowed. Since magnetizable materials are not common in the earth outside of certain types of ore bodies, μ is taken to be the free space value μ_0 everywhere. Extension of the solution for varying permeability is straightforward.

In a homogeneous material any electromagnetic field may be separated into two modes about an arbitrary direction in space, each of which satisfies (1)—(3) independently. The separation axis is taken as the direction along which conductivity varies, labeled the z axis. The transverse electric (TE) mode is marked by current loops circling the z axis and coupled to each other through the conducting medium by induction. The transverse magnetic (TM) mode consists of current loops in the plane of the z axis which cut across the changing medium properties. TE and TM modes produce no vertical electric and magnetic fields, respectively. Owing to the nonconducting atmosphere, ionospheric current systems can induce only TE modes in the earth. Sources within the conducting earth; whether artificial or natural, may produce a combination of the two modes. Note that TE modes vanish in the limit of zero frequency because inductive effects disappear, while DC currents are the limiting case of TM modes.

A Cartesian coordinate system with z positive upward, oriented in the direction of changing electrical conductivity, is used. A standard theorem of vector analysis allows the decomposition of any vector field into a combination of three scalar fields [cf. *Morse and Feschbach*, 1953, ch.13]:

$$\vec{T} = \nabla\phi + \nabla \times (\psi\hat{z}) + \nabla \times \nabla \times (\chi\hat{z}) \tag{4}$$

Using (1) and (4), the magnetic induction may be written as

$$\vec{B} = \nabla \times (\Pi\hat{z}) + \nabla \times \nabla \times (\Psi\hat{z}) \tag{5}$$

where Π and Ψ represent TM and TE modes, respectively. It should be noted that the formal Hertz vector representation is obtained by replacing Π with $\sigma\Pi$ in (5); the simpler form shown will be used.

Applying (4) to the source current $\vec{J}^0$ and separating out the vertical component explicitly yields

$$\vec{J}^0 = J_z^0\hat{z} + \nabla_h T + \nabla \times (\Upsilon\hat{z}) \tag{6}$$

where T and Υ are functions that satisfy the Poisson equations

$$\nabla_h^2 T = \nabla_h \cdot \vec{J}_h^0 \tag{7}$$

$$\nabla_h^2 \Upsilon = -(\nabla_h \times \vec{J}_h^0) \cdot \hat{z} \tag{8}$$

with appropriate boundary conditions in the presence of vertical discontinuities in $\vec{J}_h^0$. The subscript in (6)—(8) refers to the transverse components.

Differential equations for Π and Ψ are derived by substituting (5) and (6) into (2) and (3)

$$\nabla_h^2\Pi + \sigma\partial_z(\partial_z\Pi/\sigma) - i\omega\mu\sigma\Pi = -\mu J_z^0 + \mu\sigma\partial_z(T/\sigma) \tag{9}$$

$$\nabla^2\Psi - i\omega\mu\sigma\Psi = -\mu\Upsilon \tag{10}$$

where the electric field is

$$\vec{E} = \frac{1}{\mu\sigma}\nabla \times \nabla \times (\Pi\hat{z}) - \frac{1}{\sigma}(J_z^0\hat{z} + \nabla_h T) - i\omega\nabla \times (\Psi\hat{z}) \tag{11}$$

The source current has been decomposed in (6) into exactly those parts which produce TM modes, J_z^0 and $\nabla_h T$, and that part which produces a TE mode, $\nabla \times (\Upsilon\hat{z})$.

At any horizontal boundary, the usual conditions on the tangential electric and magnetic fields, the normal magnetic field, and the normal current must be satisfied. Using (5) and (11), it is easy to show that continuity of Ψ, $\partial_z\Psi$, Π, and $(1/\sigma)(\partial_z\Pi - T)$ meets these requirements.

POINT CURRENT SOLUTIONS

Solutions of (7)—(10) for either vertical or horizontal current sources serve the purpose of Green functions since the fields from an arbitrary source can be constructed from them by summation or integration. From (9) it is clear that a VED source produces only TM modes, while (9) and (10) indicate that an HED source produces both TE and TM modes. It can be shown that VMD sources induce only TE modes, while HMD sources induce only TM modes. The HED is the most general case and will be considered in detail in this paper, but the

expressions given are applicable to any of the four source types.

An artificial point source at the coordinates $(0, 0, z')$ with magnitude $p = Idl$, where I is the source current and dl is its infinitesimal length is represented by

$$J^0 = p\delta(x)\delta(y)\delta(z-z') \tag{12}$$

where δ is the Dirac delta function. General horizontal location of the source will be considered later.

Equations (9) and (10) are most easily solved by using the Bessel transform pair

$$\hat{f}(k,z) = \int_0^\infty d\rho\, J_0(k\rho)\rho f(\rho,z)$$
$$f(\rho,z) = \int_0^\infty dk\, J_0(k\rho)k\hat{f}(k,z) \tag{13}$$

where J_0 is the Bessel function of the first kind of order zero. The parameter k is analogous to the wave number in the Fourier integral, and (13) is formally equivalent to a double Fourier transform.

Applying (13) to (9) with (12) for a vertical current source ($T = Y = 0$) yields

$$\sigma\partial_z(\partial_z\hat{\Pi}_v/\sigma) - \beta^2\hat{\Pi}_v = -\frac{\mu p}{2\pi}\delta(z-z') \tag{14}$$

where

$$\beta(z) = \sqrt{k^2+i\omega\mu\sigma(z)} \tag{15}$$

This is solved by the usual variation of parameters method to give

$$\Pi_v(\rho,z,\omega) = \frac{\mu p}{2\pi}\int_0^\infty dk\, J_0(k\rho)k\,\frac{\sigma(z)}{\sigma(z')}\,U_1(z_>)U_2(z_<) \tag{16}$$

where U_1 and U_2 satisfy the homogeneous form of (14), the boundary conditions $U_1 = 0$ as $z \to \infty$, $U_2 = 0$ as $z \to -\infty$, and the Wronskian condition $W(U_1, U_2) = 1$. The subscripts on z refer to the larger or smaller of the field point z and the source point z'.

The horizontal current source requires solutions of (7) and (8). We consider a point current oriented along the y axis ($\phi' = 0$); the conjugate solution is straightforward. Substituting (12) into (7), solving for T, using a Green function for (9), and integrating by parts yields the TM mode solution

$$\Pi_h(\rho,z,\omega) = -\frac{\mu p}{2\pi}\partial_x\int_0^\infty dk\, J_0(k\rho)\,\frac{1}{k}\,\frac{\sigma(z)}{\sigma(z')}\cdot\partial_{z'}[U_1(z_>)U_2(z_<)] \tag{17}$$

where U_1 and U_2 were defined for (16). Substituting (11) into (8), finding Y, and solving gives

$$\Psi(\rho,z,\omega) = -\frac{\mu p}{2\pi}\partial_y\int_0^\infty dk\, J_0(k\rho)\,\frac{1}{k}\,V_1(z_>)V_2(z_<) \tag{18}$$

where V_1 and V_2 are analogous to U_1 and U_2. Note that (17) and (18) are azimuth dependent, while (16) is independent of azimuth, as would be expected from symmetry considerations. Note also that the VED and HED produce functionally different TM modes.

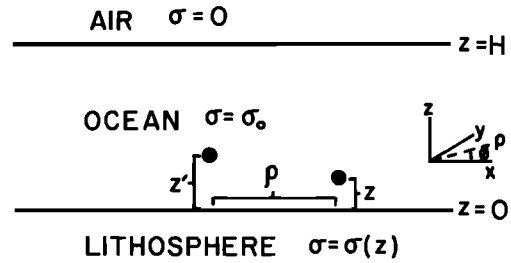

Fig. 1. Geometry used in the mathematical derivations. The source is located a distance z' above the seafloor ($z = 0$), while the receiver is at a horizontal distance ρ and a height z. The ocean has a uniform conductivity of σ_0, and the lithospheric conductivity $\sigma(z)$ is dependent only on depth. The ocean depth H is taken as infinite in the text, and the finite depth case is treated in Appendix A.

Since (13) separates the vertical and horizontal coordinate dependence of the solution, generalization of (16)–(18) for a source at (ρ', ϕ', z') follows from the geometry by replacing ρ in (16)–(18) with

$$\zeta = \sqrt{\rho^2+\rho'^2-2\rho\rho'\cos(\phi-\phi')} \tag{19}$$

It should be noted that a Bessel function with argument (19) can be expanded into a series of products of Bessel functions and trigonometric functions [*Watson*, 1962]. This yields the formal eigenfunction expansion solution of (9) and (10).

THE ELECTROMAGNETIC FIELDS

The electrical conductivity of seawater is almost entirely a function of temperature and salinity, with a very small pressure effect [*Horne and Frysinger*, 1963]. In the ocean the gross thermal and salinity structure consists of a thin surface layer of warm water separated from a thick, cold water mass by the main thermocline. The subthermocline ocean has a nearly uniform electrical conductivity of 3.2 S/m. In this section the ocean will be modeled as a uniform half space. This is a good approximation except in shallow water or at very low frequencies (<0.05 Hz) when the source is located near the seafloor. The complete solution for an HED source, including the effect of internal reflections from a thermocline or the sea surface, is contained in Appendix A. For simplicity the treatment here is limited to a point source; again the complete solution is in the appendix. Figure 1 illustrates the geometry.

Point source solutions for the electromagnetic potentials Π and Ψ are found by combining (16)–(18) for a uniform whole space with solutions of (9) and (10) without sources and including the boundary conditions at the seafloor. Two electromagnetic response functions, analogous to the magnetotelluric response function, contain all of the information on suboceanic conductivity. They are defined as

$$\Lambda = \left.\frac{\Psi}{\partial_z\Psi}\right|_{z=0} \tag{20}$$

$$K = \left.\frac{\sigma\Pi}{\partial_z\Pi}\right|_{z=0} \tag{21}$$

where Λ corresponds to TE modes and K to TM modes. Methods for their computation are derived in the next section. The three potential functions for vertical and horizontal current sources are

$$\Pi_v(p,z,\omega) = a\int_0^\infty dk\, J_0(kp)\,\frac{k}{\beta_0}\left[R_{TM}e^{-\beta_0(z+z')}+e^{-\beta_0|z-z'|}\right] \quad (22)$$

$$\Pi_h(p,z,\omega) = a\,\partial_x\int_0^\infty dk\, J_0(kp)\,\frac{1}{k}\left[R_{TM}e^{-\beta_0(z+z')}\mp e^{-\beta_0|z-z'|}\right] \quad (23)$$

$$\Psi(p,z,\omega) = -a\,\partial_y\int_0^\infty dk\, J_0(kp)\,\frac{1}{k\beta_0}\left[R_{TE}e^{-\beta_0(z+z')}+e^{-\beta_0|z-z'|}\right] \quad (24)$$

where $a = \mu p/4\pi$ and β_0 is given by (15) with $\sigma = \sigma_0$, the conductivity of the ocean half space. The upper sign in (23) holds for $z > z'$ and vice versa. R_{TE} and R_{TM} are analogs of the reflection coefficients of electromagnetic wave theory, where

$$R_{TE} = \frac{\beta_0\Lambda-1}{\beta_0\Lambda+1} \quad (25)$$

$$R_{TM} = \frac{\beta_0 K/\sigma_0-1}{\beta_0 K/\sigma_0+1} \quad (26)$$

Each of (22)—(24) holds for a point source located at the coordinate system origin, and the general case is obtained by substituting (19) for ρ in the Bessel functions.

The electromagnetic fields are obtained by applying (5) and (11) to (22)—(24). For the VED only three nonzero electromagnetic components exist.

$$E_\rho = b\int_0^\infty dk\, J_1(kp)k^2\left[R_{TM}e^{-\beta_0(z+z')}\pm e^{-\beta_0|z-z'|}\right] \quad (27)$$

$$E_z = b\int_0^\infty dk\, J_0(kp)\,\frac{k^3}{\beta_0}\left[R_{TM}e^{-\beta_0(z+z')}+e^{-\beta_0|z-z'|}\right] \quad (28)$$

$$B_\phi = a\int_0^\infty dk\, J_0(kp)\,\frac{k^2}{\beta_0}\left[R_{TM}e^{-\beta_0(z+z')}+e^{-\beta_0|z-z'|}\right] \quad (29)$$

where $b = p/4\pi\sigma_0$. The horizontal source current produces all six electromagnetic field components

$$E_\rho = c\left[\int_0^\infty dk\left[I(k\rho)\beta_0 R_{TM}-\frac{J_1(kp)}{\rho}\,\frac{\gamma_0^2}{\beta_0}R_{TE}\right]e^{-\beta_0(z+z')}\right.$$
$$\left.-\int_0^\infty dk\left[J_0(kp)k\beta_0-\frac{J_1(kp)}{\rho}\,\frac{k^2}{\beta_0}\right]e^{-\beta_0|z-z'|}\right] \quad (30)$$

$$E_\phi = -d\left[\int_0^\infty dk\left[\frac{J_1(kp)}{\rho}\beta_0 R_{TM}-I(kp)\,\frac{\gamma_0^2}{\beta_0}R_{TE}\right]e^{-\beta_0(z+z')}\right.$$
$$\left.+\int_0^\infty dk\left[J_0(kp)\,\frac{k}{\beta_0}\gamma_0^2+\frac{J_1(kp)}{\rho}\,\frac{k^2}{\beta_0}\right]e^{-\beta_0|z-z'|}\right] \quad (31)$$

$$E_z = -c\int_0^\infty dk\, J_1(kp)k^2\left[R_{TM}e^{-\beta_0(z+z')}\mp e^{-\beta_0|z-z'|}\right] \quad (32)$$

$$\beta_\rho = e\left[\int_0^\infty dk\left[\frac{J_1(kp)}{\rho}R_{TM}-I(kp)R_{TE}\right]e^{-\beta_0(z+z')}\right.$$
$$\left.\pm\int_0^\infty dk\, J_0(kp)ke^{-\beta_0|z-z'|}\right] \quad (33)$$

$$B_\phi = f\left[\int_0^\infty dk\left[I(kp)R_{TM}-\frac{J_1(kp)}{\rho}R_{TE}\right]e^{-\beta_0(z+z')}\right.$$
$$\left.\mp\int_0^\infty dk\, J_0(kp)ke^{-\beta_0|z-z'|}\right] \quad (34)$$

$$B_z = e\int_0^\infty dk\, J_1(kp)\,\frac{k^2}{\beta_0}\left[R_{TE}e^{-\beta_0(z+z')}+e^{-\beta_0|z-z'|}\right] \quad (35)$$

where $c = b\cos\phi$, $d = b\sin\phi$, $e = a\sin\phi$, $f = a\cos\phi$, $\gamma_0^2 = i\omega\mu\sigma_0$ and

$$I(kp) = kJ_0(kp) - \frac{J_1(kp)}{\rho} \quad (36)$$

In each of (27)—(35) the last terms may be evaluated analytically (Appendix B). Separate expressions for the TE and TM mode parts of the horizontal source fields can also be obtained.

The mathematical complexity of (27)—(35) masks their conceptual simplicity. In each case the first terms, involving the coefficients R_{TE} and R_{TM}, represents the electromagnetic field due to an image current induced in the conducting earth, while the second terms represent the primary field in the ocean. In contrast to the terrestrial case, the primary fields attenuate rapidly with range from the source or with increasing frequency (see Appendix B). Note that the vertical source fields are independent of azimuth, while the horizontal source fields display simple trigonometric dependence. The vertical field expressions (32) and (35) represent only TM or TE modes, as they must by definition. Note also that increasing vertical separation of either the source or receiver from the sea floor results in both rapid attenuation of the fields and decreased spatial resolution of its features due to the wave number dependence of the exponential.

Edwards et al. [1981] considered a VED source consisting of an insulated wire stretching from the seafloor to the sea surface. For this situation the sea surface is important, and (22) and (27)—(29) must be modified to include a reflected wave and integrated over the extent of the source to model it. For an HED, the finite length of real sources is important for observation points near the source. At very low frequencies, surface and thermocline reflections will influence the received fields.

NUMERICAL METHODS

Approximate or asymptotic solutions of electromagnetic problems in a half space over certain ranges of ρ, z, ω, and σ are available in the literature [cf. *Wait*, 1961; *Keller*, 1968]. The treatment of a more general conductive struc-

ture cannot be accomplished with analytic methods, and numerical evaluation of the integrals must be applied.

Integrals like (27)–(35), whose integrand consists of a Bessel function $J_\nu(kp)$ multiplying a kernel function $K(k)$, are ubiquitous in physical problems involving cylindrical symmetry. Owing to the diffusion nature of (1)–(3), the kernel functions for electromagnetic induction are smoothly varying with wave number k, in contrast to the nearly discontinuous kernels that occur in seismological problems. This property has been exploited in the digital convolution method of evaluation [*Anderson*, 1979], which yields adequate results for a restricted range of horizontal distance and frequency. The TE and TM modes for the HED are of similar amplitude but are asymptotically out of phase as frequency increases. If they are to be calculated explicitly, an algorithm with more precision than that of *Anderson* [1979] must be used.

Direct numerical integration was employed to solve (27)–(35) numerically. The integral was evaluated between the zero crossings of the Bessel functions by adaptive quadrature [*Patterson*, 1973]. The series of partial integrations is, in general, slowly convergent or even divergent, and the Padé approximants to the sum were used to force convergence. The result yields double precision computer accuracy at a slight cost in computer time. Details and a computer program are available from the first author.

Computation of the electromagnetic fields (27)–(35) requires the evaluation of the response functions (20) and (21). These may be obtained in two ways. A suitable transformation exists to convert the homogeneous form of the Bessel transforms of (9) and (10) into Ricatti equations for the response functions

$$\partial_z \Lambda + \beta^2 \Lambda^2 = 1 \tag{37}$$

$$\sigma \partial_z K + \beta^2 K^2 = \sigma^2 \tag{38}$$

These are easily solved for any $\sigma(z)$ by standard numerical methods. It is common in geophysics to model the earth as a stack of layers of varying thickness and conductivity. Recursion relations for (20) and (21) can be derived and expressed as continued fractions

$$\Lambda = Q_1 + \cfrac{q_1^2 - Q_1^2}{Q_1 + Q_2 + \cfrac{q_2^2 - Q_2^2}{\vdots \cfrac{}{Q_{N-1} + Q_N}}} \tag{39}$$

$$K = R_1 + \cfrac{r_1^2 - R_1^2}{R_1 + R_2 + \cfrac{r_2^2 - R_2^2}{\vdots \cfrac{}{R_{N-1} + R_N}}} \tag{40}$$

where $q_j = 1/\beta_j$, $Q_j = \coth(\beta_j h_j)/\beta_j$, $r_j = \sigma_j/\beta_j$, $R_j = \sigma_j \coth(\beta_j h_j)/\beta_j$. The layered structure terminates in a half space.

Electromagnetic Response of the Ocean Lithosphere

In this section the electromagnetic response of simple models of the ocean and ocean lithosphere will be explored. The purpose of the analysis is both to gain some insight into the behavior of the electromagnetic fields in the presence of conductive structure and to place some broad constraints on the experimental variables—source frequency and source-receiver range—that are used in actual measurements. In all cases the earth is modeled as a stack of layers for computational and conceptual simplicity.

The VED source will not be considered further since *Edwards et al.* [1981] have discussed it in depth. It should be noted that the electromagnetic fields generated by a VED are both weaker by a factor of at least 100 for a given range and frequency and attenuate more rapidly with range when compared to those from an HED with the same source strength. This is caused by reduced coupling of the VED electromagnetic fields to the low dissipation rock and suggests that much deeper penetration will be obtained using the HED source.

The electrical conductivity of seawater varies between 3.2 and 5 S/m, with the higher value occurring in the warm, near-surface waters. The ocean will be treated as a uniform half space with a conductivity of 3.2 S/m in most of the models of this section. By contrast, the electrical conductivity of the crust and mantle has not been measured extensively, particularly the less accessible zone below seismic layer 2. A model for the crust will be presented which suggests that the highest electrical conductivity normally occurs near the surface. The large-scale resistivity experiment on DSDP leg 70 indicates a mean value of 0.1 S/m for the layer 2 pillow basalts on very young lithosphere [*von Herzen et al.*, 1981]. Downhole electrical logs in this hole yield a similar value when properly averaged (Appendix C). Logs in other holes suggest a decrease in conductivity by a factor of 3 as the crust ages from 0 to 10 m.y. In this section the entire lithosphere will be modeled as a half space of conductivity 0.05 S/m, near the upper crustal value. This should be regarded as an upper limit and is useful for estimating minimum field amplitudes and in demonstrating sensitivity to buried structure.

Figure 2 illustrates the general behavior of the electromagnetic fields generated by artificial sources in the ocean. The plot shows the phase and amplitude of the horizontal electric field as a function of source frequency from 0.01 to 100 Hz and range from 1 to 5 km. The point source is assumed to have unit amplitude (i.e., a 1 a-M dipole moment) and is located 1 m above the seafloor. Measurements are made at the seafloor at various horizontal ranges. The azimuth is 0° (the electric field vector in the direction of the wire source is measured). The experimental apparatus discussed by *Cox et al.* [1981] consists of a 0.8-km wire carrying 75 A, so that actual field amplitudes would be 6×10^4 times larger than shown.

The electromagnetic skin depths at 1 Hz are 280 m in seawater and 2.3 km in the lithosphere for the parameters used. Propagation through the ocean is significant only for the lowest frequencies and ranges in Figure 2, and most of the attenuation is controlled by the lithospheric conductivity. At ranges much smaller than a skin depth, the field amplitudes and phases are nearly independent of frequency. This is commonly called the quasi-static zone. At ranges much larger than a skin depth the electric field phase and amplitude decrease rapidly with both frequency and range. This is the far-field zone; note that most of the values shown in Figure 2 are located in the very far field for propagation in seawater. In between these

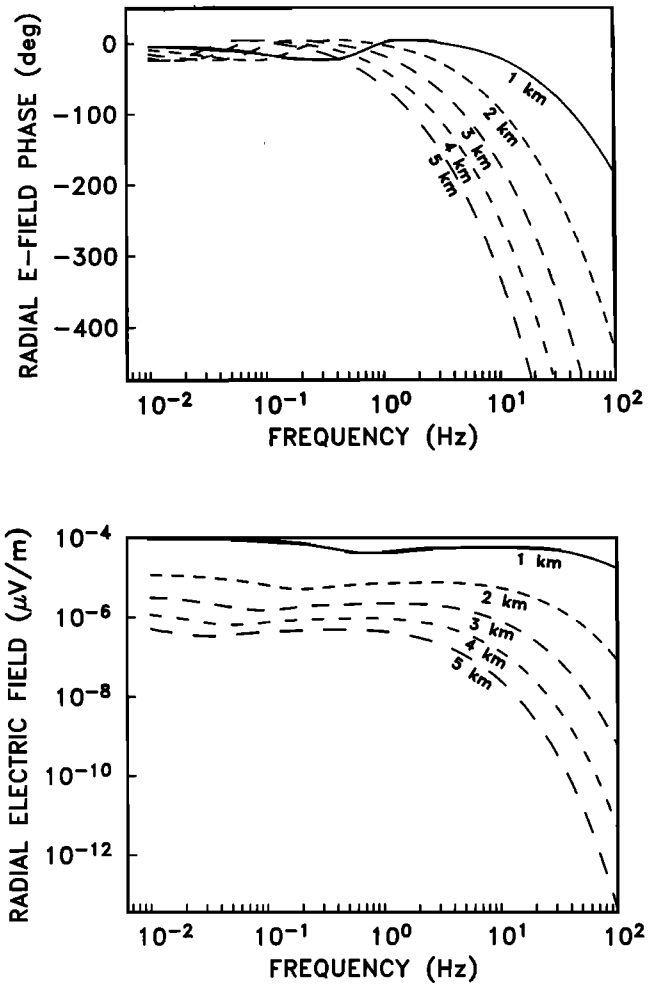

Fig. 2. The radial electric field phase and amplitude at an azimuth of 0° for a point source as a function of frequency and range. The ocean half space is assumed to have a conductivity of 3.2 S/m, while the lithosphere half space has a conductivity of 0.05 S/m. The source is located 1 m above the seafloor, where the observations are made. The units of E are $\mu V/m$ and of B are nT and the source strength is 1 A m.

extremes at ranges of the order of one skin depth in the lithosphere the near field is encountered and is the region where significant attenuation and dispersion of the electromagnetic fields begins to be manifest.

Figure 3 shows the phase and amplitude for the horizontal magnetic field as a function of source frequency from 0.01 to 10 Hz and range from 1 to 5 km. The remaining model parameters are as for Figure 2, although the magnetic field component is oriented at right angles to the electric field component. Qualitative similarity is apparent, but the decrease in field amplitude with frequency and range is slower, as is expected from the asymptotic theory [*Wait*, 1961].

Figure 4 compares the horizontal and vertical electric and magnetic fields as a function of range at a frequency of 1 Hz with an azimuth of 0° for the electric field and 90° for the magnetic field. In both cases the vertical field amplitudes are smaller by at least an order of magnitude, and the difference increases with range as the vertical field attenuates more rapidly. In the near to far field the phase decreases at a rate of about 1 rad per skin depth in the lithosphere (2.3 km), and the amplitude decreases nearly exponentially in the far field. In the quasi-static zone both the phases and amplitudes are nearly independent of range. From Figures 2—4 it is clear that measurement of the horizontal field components is preferred using an HED source. By the reciprocity theorem of electromagnetism, the dashed curves in Figure 4 are equivalent to the horizontal fields produced by a VED, illustrating the advantage of a horizontal source.

Since any practical transmitter antenna will have an appreciable length, the point source model has errors associated with it. Figure 5 displays the fractional difference for a point source and a 1-km-long wire with an identical moment. The azimuth is 0°. Since the observation point and wire are closest for this azimuth, this should be regarded as a worst case calculation. For both the electric and magnetic field components, the point source is an excellent approximation at ranges greater than a skin depth in the lithosphere (2.3 km for the case shown). The error rises very rapidly at shorter ranges, especially in the electric field, and is infinite at the origin. Figure 5 suggests that Figures 2 and 3 are seriously in error at their respective low-frequency limits, but the phase effect is much smaller.

Figure 6 shows the effect that a finite depth ocean has on the horizontal electric and magnetic fields. In both cases the ocean half-space model is compared to a 1-km-

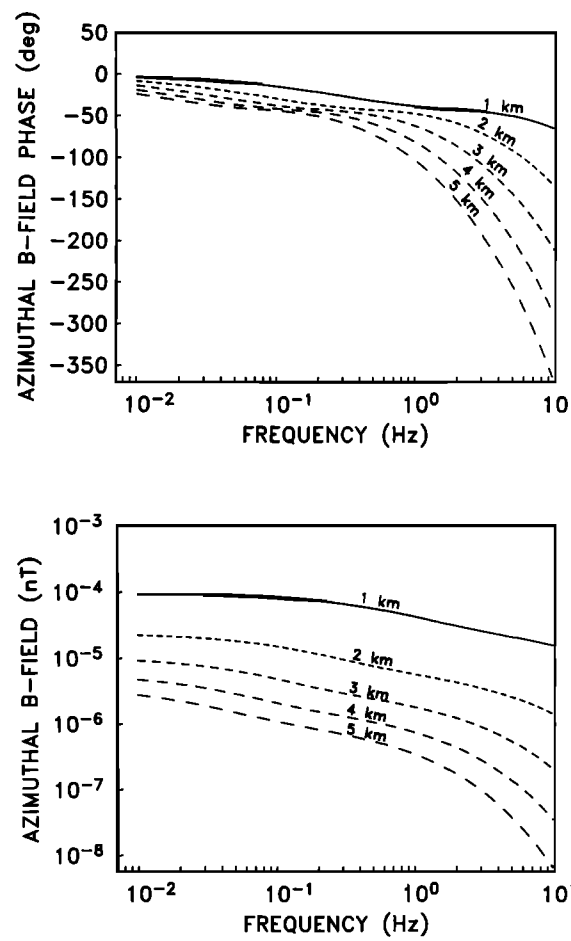

Fig. 3. The azimuthal magnetic field phase and amplitude at an azimuth of 0° as a function of source frequency and range. See Figure 2 caption for details.

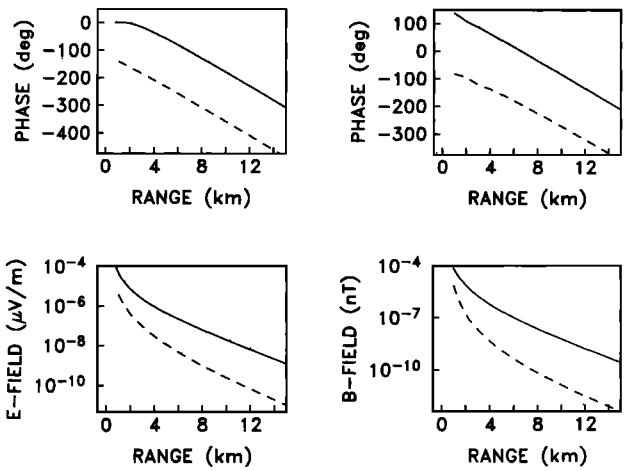

Fig. 4. The radial (solid line) and vertical (dashed line) electric field phase and amplitude at an azimuth of 0° (left panels) and the radial (solid line) and vertical (dashed line) magnetic field phase and amplitude at an azimuth of 90° (right panels) as a function of range. See Figure 2 caption for details of the other parameters.

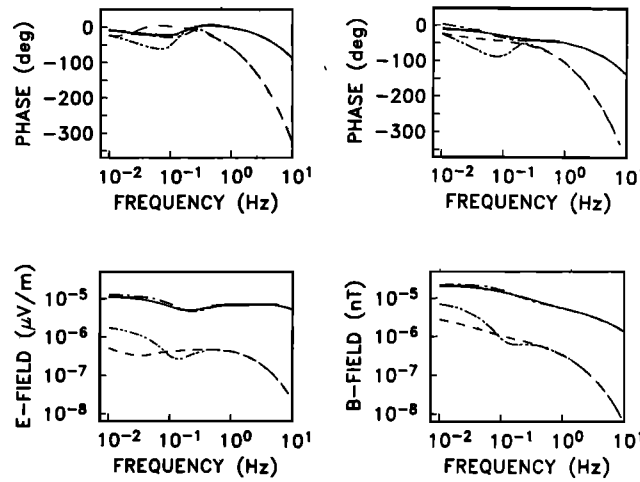

Fig. 6. The electromagnetic response for an ocean of depth H = 1 km compared to the infinite depth model for the radial electric field (left panels) and azimuthal magnetic field (right panels) for an azimuth of 0°. The half-space ocean at 2 km (solid line) and 5 km (dashed line) and the 1 km ocean at 2 km (dot-dashed line) and 5 km (double dot-dashed line) are shown. See Figure 2 caption for other details.

deep ocean at source-receiver ranges of 2 and 5 km. Differences are observed at frequencies where the water column represents a few skin depths or less, and the effect increases with source-receiver separation. The influence of destructive and constructive interference from surface reflections is seen and is most severe for the electric field. Inclusion of a higher-conductivity region above the main thermocline produces response curves qualitatively similar to those shown.

Figures 7 and 8 illustrate the sensitivity of the controlled source electromagnetic fields to a thin conductive or resistive zone at depth. For the first figure a 100-m-thick, 0.25-S/m layer is buried at 1 km in a 0.05-S/m half space, while for the second case a low conductivity of 0.005 S/m is used. The choice of layer thicknesses and depths is arbitrary but serves to show the different effects of high- and low-conductivity material. Since electromagnetic waves in conducting media attenuate and disperse with distance, the qualitative effect of deeper conductivity changes will be similar to that shown but with reduced amplitude.

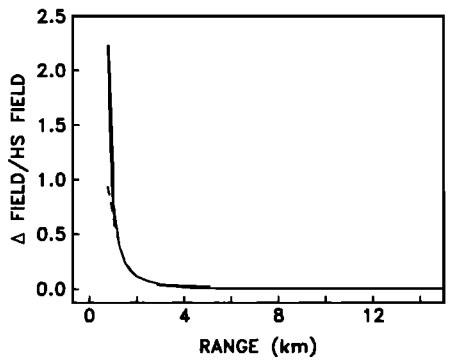

Fig. 5. The fractional difference between the finite and point source calculations for the radial electric (solid line) and azimuthal magnetic (dashed line) components as a function of range at a frequency of 1 Hz. See Figure 2 caption for other parameters. The fractional difference is the quantity (finite field—point field)/point field.

It is quite apparent that the fields are preferentially sensitive to low-conductivity material. The amplitude change shown in Figure 8 is an order of magnitude larger than that of Figure 7, and the phase shifts are also bigger. At a fixed source-receiver range an initial decrease in amplitude is followed by a larger increase as frequency rises for the high-conductivity case. The sense of the field change is reversed for the low-conductivity material. This pattern repeats in an oscillatory manner at higher frequencies and is the result of internal trapping of electromagnetic energy. Note that a larger range is required to produce amplitude change for the low-conductivity zone, but the phase does change significantly at shorter separations. The magnetic field is only slightly less sensitive to structure as compared to the electric field.

CONDUCTIVITY MODEL OF THE OCEAN CRUST

As noted previously, the ocean crust must exhibit a decrease in electrical conductivity beneath seismic layer 2 to explain the results obtained by *Young and Cox* [1981], and more detailed conductivity models will be considered based on field and laboratory data. Our knowledge of typical ocean crustal and mantle structure comes from terrestrial ophiolite exposures and deep ocean seismic studies. The most thoroughly studied ophiolites are those in Oman [*Coleman*, 1981] and Newfoundland [*Salisbury and Christensen*, 1978]. The petrological and seismic structures of these rocks are in gross agreement with those obtained in the present day ocean if allowance for weathering of the ophiolites is made. From the seafloor down the ocean crustal structure exhibits (1) sediments whose thickness depends on plate age, tectonic setting, biological productivity, and chemical dissolution, (2) basalts of both fractured flow and pillow types with a total thickness of 0.5 to 1.5 km, (3) feeder dykes showing extensive fracturing in the uppermost part, grading into a solid sheeted dyke layer several hundred meters thick, (4) a gabbro layer 3—5 km thick showing a petrological gradation diagnostic of multi-

ple plutonic events [*Pallister and Hopson*, 1981], and (5) an abrupt transition to peridotite depleted of basalt-forming minerals. This interface is widely believed to coincide with the seismic Mohorovicic discontinuity.

The basalts from ophiolite sequences have undergone profound hydrothermal alteration, especially in the pillow layers, and fractures are often filled with clay minerals and calcite. This process probably occurs at the seafloor and causes the gradual conductivity decrease with age inferred from DSDP electric logs as the closing of cracks reduces the effect of fluid conduction. The deeper gabbro layers display both low and moderately high temperature hydrothermal alteration, the latter associated with interaction of the rock with a small volume (around twice the rock volume) of seawater [*Gregory and Taylor*, 1981]. The low-temperature alteration, in which olivine is transformed to serpentine, is problematical and may be either subaerial or a consequence of the obduction process. The subcrustal peridotite undergoes very limited high-temperature alteration [*Gregory and Taylor*, 1981], but low-temperature serpentinization is frequently observed.

Conductivity in rocks at subsolidus temperatures is dominated by the effects of interstitial fluids at low temperatures [*Shankland and Waff*, 1974] and thermally activated mineral conduction at higher temperatures [*Shankland*, 1975]. By combining the field observations with laboratory data on basalts and ultramafic rocks [*Rai and Manghnani*, 1977, 1978], the following conductivity model of the ocean crust is proposed:

1. Sediments—The conductivity is estimated from Archie's law as a function of porosity and varies from 0.01 S/m in indurated materials to 2.5 S/m for fresh, seawater-saturated sediments. The sediment layer is rarely more than a few hundred meters thick.

2. Basalt (layer 2)—The bulk conductivity of young, fractured basalt is near 0.1 S/m [*von Herzen et al.*, 1981].

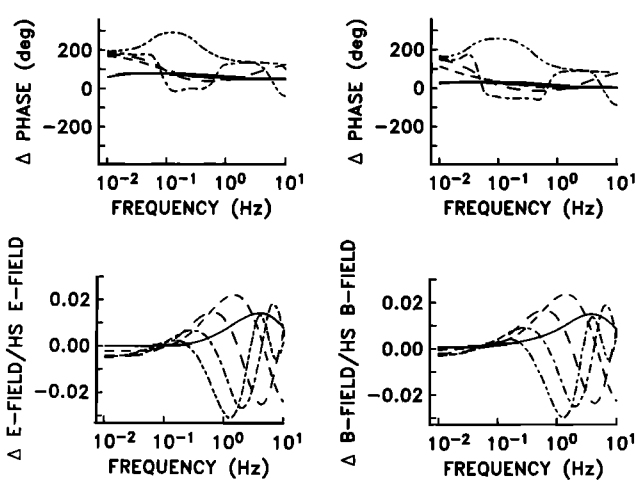

Fig. 7. The phase difference and fractional amplitude change for a conductivity model consisting of a half space of conductivity 0.05 S/m containing a 0.25-S/m layer 100 m thick buried at 1 km overlain by a 3.2 S/m ocean half space. The radial electric field (left panels) and azimuthal magnetic field (right panels) at an azimuth of 0° are shown as a function of source frequency and ranges of 1 km (solid line), 2 km (short dashed line), 3 km (long dashed line), 4 km (dot-dashed line), and 5 km (double dot-dashed line).

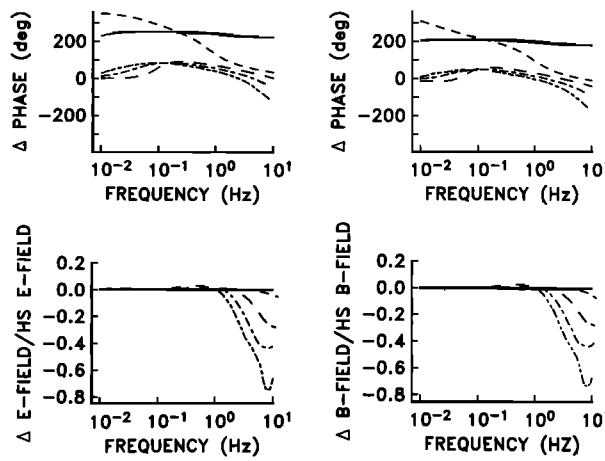

Fig. 8. Same as for Figure 7 with the 0.25-S/m layer replaced by a low conductivity 0.005 S/m layer.

At an age near 10 m.y., weathering lowers this to 0.035 S/m by the closing of cracks and pores.

3. Feeder dykes and gabbros (layer 3)—The conductivity probably decreases to a low value of 0.003 S/m. The estimates of *Young and Cox* [1981] show that counterbalancing effects tend to keep the conductivity constant with plate age. As the gabbro cools, cracking permits the entry of seawater, keeping the upper part of this layer more highly conducting. In the lower parts of newly formed layer 3 gabbros this mechanism is less important due to temperatures in excess of 400°C, where fluid ionic mobility is reduced, but mineral conductivity mechanisms do become important. If the temperature is low enough, the lower part of the gabbro unit could have a conductivity of 0.001 S/m, and higher temperature, as on young crust, may raise this by a factor of 10. The possible presence of serpentine minerals from low-temperature alteration makes for even greater uncertainty, as this material can be as conductive as 0.01 S/m or more [*Stesky and Brace*, 1973].

4. Peridotite—Below the Moho the electrical conductivity is probably lower than in the gabbro layer because of reduced hydrothermal activity, lower water content, and the absence of conductive mineral phases. The bulk conductivity may be around 0.0004 S/m in the top 20 km of the mantle, but this is quite uncertain. For example, aseismic ridges exhibit low upper mantle seismic velocities which may result from extensive serpentinization [*Chave*, 1979; *Souriau*, 1981]; this would increase the conductivity markedly.

Figure 9 summarizes the ocean crust model.

The electromagnetic response of two ocean crust models were examined and appear as Figures 10 and 11. The left panel of both figures corresponds to a model with a 0.05-S/m basalt layer 1 km thick, a 0.003-S/m dyke and gabbro layer 2.5 km thick, and a 0.001-S/m lower crustal layer 2 km thick, underlain by a mantle half space of conductivity 0.0005 S/m. The right panel model differs only in the lower crust layer, where the conductivity is 0.01 S/m, and represents young, hot crust, while the first case represents older material. Figure 10 shows the horizontal electric field at ranges of 4, 10, and 16 km from the source. Departure from the half-space behavior of Figure 2 is

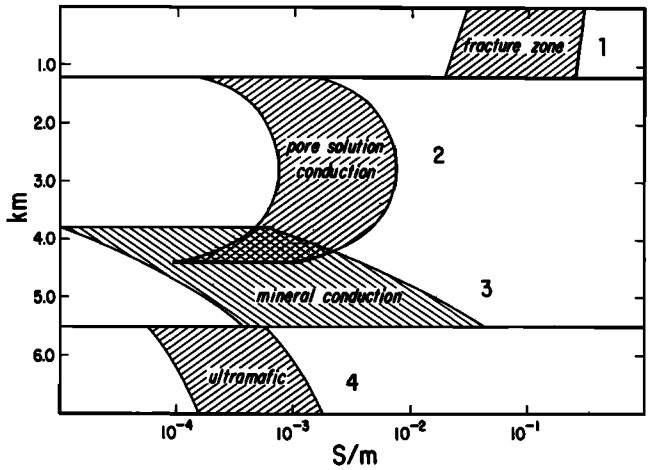

Fig. 9. Electrical conductivity model of the ocean crust and upper mantle derived from petrological, geological, and laboratory data. See text for details.

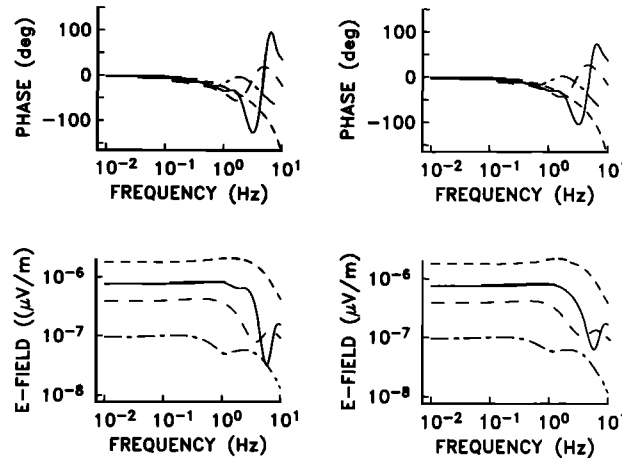

Fig. 11. The models of Figure 10 are shown at ranges of 3 km (short dashed line), 4 km (solid line), 5 km (long dashed line), and 8 km (dot-dashed line). See Figure 10 caption for details.

obvious, and marked phase differences between the two crust models are observed at long source-receiver separations. Figure 11 shows the same two models at ranges of 3, 4, 5, and 8 km. Amplitude and phase differences are large, especially at 4 km and high frequencies. This variation is caused by the deep crustal layer, and the active source method is capable of detecting differences in structure at such depths.

Discussion

The models presented in the last two sections show that (1) the HED source is preferred to the VED source for sounding the suboceanic lithosphere, (2) the horizontal electromagnetic components rather than their vertical counterparts are the best measurement variable, (3) the finite size of real sources is important at short source-receiver separations, (4) the effect of reflections off of the sea surface will be important at large source-receiver separations, low frequencies, or in relatively shallow water, and (5) the choice of transmitter and receiver locations and source frequencies will affect the resolution ability of actual data. Of these points, 3 and 4 are easily incorporated into the theory if both water depth and source location are accurately determined. The former is accomplished by acoustic ranging on transponders located at the ends of the transmitter antenna.

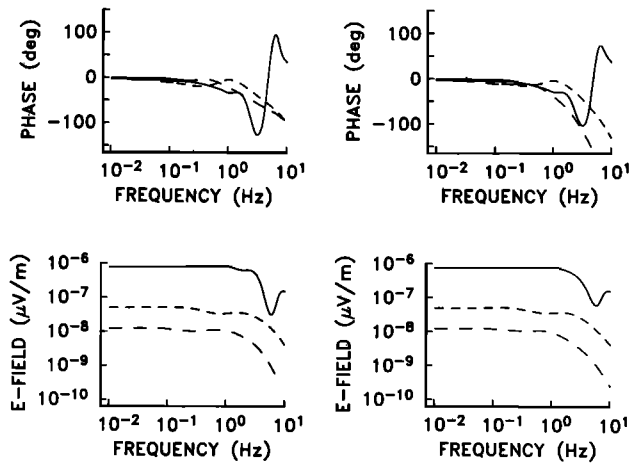

Fig. 10. The radial electric field response for two ocean crust models shown as a function of frequency at ranges of 4 km (solid line), 10 km (short dashed line), and 16 km (long dashed line). The left panels represent cold crust consisting of a 0.05-S/m layer 2 basalt layer 1 km thick, a 0.003-S/m dike and gabbro layer 2.5 km thick, and a 0.001-S/m lower crust layer 2 km thick overlying a 0.0005-S/m half space. The right panels represent young, hot crust, and the lower crust layer has a conductivity of 0.01 S/m. The source is located 1 m above the seafloor, where measurements are made, and the point dipole approximation is used.

Figures 7—8 and 10—11 show that deep structure does influence the electromagnetic fields at all ranges and over a wide band of frequencies. The choice of these parameters is structure dependent and will influence the resolution ability of the data. Quantitative assessment of this will be deferred to a subsequent paper, but some guidelines can be inferred from the models. Since electromagnetic induction is a diffusive process, data collected at long ranges will reflect an average conductivity over a greater depth zone than for shorter source-receiver spacings. This is clearly reflected in Figures 10 and 11, where the sharpest changes in the electric field amplitude occur at 4 km and the variation is progressively smoother at longer ranges. This suggests that the result of *Young and Cox* [1981] is an average value for the crust and upper mantle. The conductivity value they infer (0.004 S/m) is in the middle of the range postulated in the last section.

The selection of the measurement variable—horizontal electric or magnetic field—must be based on sensitivity, noise level, and instrumental considerations. It is useful to estimate the ambient noise power at the seafloor produced by natural electromagnetic sources. Three major components—ionospheric currents, microseisms and the nonlinear interference of surface wind waves, and direct production of electromagnetic fields by surface wind waves and swell—can be identified. Ionospheric power levels were measured by *Wertz and Campbell* [1976] on land at frequencies between 0.003—3 Hz and shown to display a rough f^{-3} dependence. Attenuation of these externally produced fields as they propagate through the conducting ocean follows an exponential law

$$S^{(\omega)}_{\text{seafloor}} = e^{-\sqrt{2\omega\mu\sigma}\,H}\, S^{(\omega)}_{\text{surface}} \tag{41}$$

where S is the power spectral density of the magnetic field, ω is the angular frequency, σ is the conductivity of seawater, and H is the water depth. Magnetic field values are converted to electric field values using the usual electromagnetic impedance relation. Microseisms, the nonlinear interference of surface wind waves, and seismic waves are treated by *Cox et al.* [1978] and *Webb and Cox* [1982]. The latter two effects are local phenomena that may be transient, but microseisms produce a broad, steady state increase of the electromagnetic power level centered near 0.2 Hz. Oceanographic noise is generated by surface wind waves, swell, and turbulence. The former two quantities can be estimated by combining the electromagnetic field amplitudes given by *Larsen* [1971] or *Chave* [1982] with the Pierson-Moskowitz wind wave power spectrum [*Phillips*, 1977].

$$E(f) = \frac{\alpha g^2}{(2\pi)^4 f^5}\, e^{-0.74(f/f_m)^{-4}} \tag{42}$$

where E is the wave amplitude variance spectrum in m^2/Hz, g is the acceleration of gravity, f is the frequency, f_m is the peak frequency where the phase velocity of a gravity wave equals that of the wind producing it, and α is a dimensionless semiempirical constant with a value near 0.001. Additional oceanographic noise is produced by turbulence. The magnetic effect is very small and the electric field is of order $\bar{V} \times \bar{F}$, where $\bar{V}$ is the turbulent velocity [*Cox et al.*, 1970]. Since turbulence is a local phenomena, its electric field influence can be reduced arbitrarily by increasing the length of the receiver antenna.

Figure 12 shows estimates of the noise level from ionospheric currents, microseisms, and wind waves and swell in water of 100 m, 1 km, and 5 km depth. Ionospheric noise is the most important contributor, and attenuation by the ocean is apparent at high frequencies in deep water. It is unlikely that frequencies below 0.05 Hz will be usable due to ionospheric contamination. Microseisms are a basin wide, depth-independent phenomenon that produce the peak between 0.1 and 1 Hz in Figure 12 by the large-scale, nonlinear interference of surface wind waves. The same mechanism can produce peaks in the power spectrum at twice the frequency of local wind waves with an amplitude that depends on the sea state. Swell is important only in shallow water at low frequencies, and the signal produced by it is more than 10 orders of magnitude smaller in 1 km of water. Note that the magnetic field is more affected by swell noise, while direct induction by wind waves is negligible.

Figures 7 and 8 show that the sensitivity of the electric field to structure is marginally better than that of the magnetic field. Figures 2, 3, and 12 predict a higher signal-to-noise ratio for the electric field. *Cox et al.* [1981] compared the performance of electrode-type electric field instruments to fluxgate, induction coil, and cryogenic magnetometers. Only the superconducting unit promises better performance than silver-silver chloride electrodes, but the cost and engineering problems make use of the cryogenic magnetometer difficult. The horizontal electric field does offer slight advantages over the magnetic field for controlled source experiments.

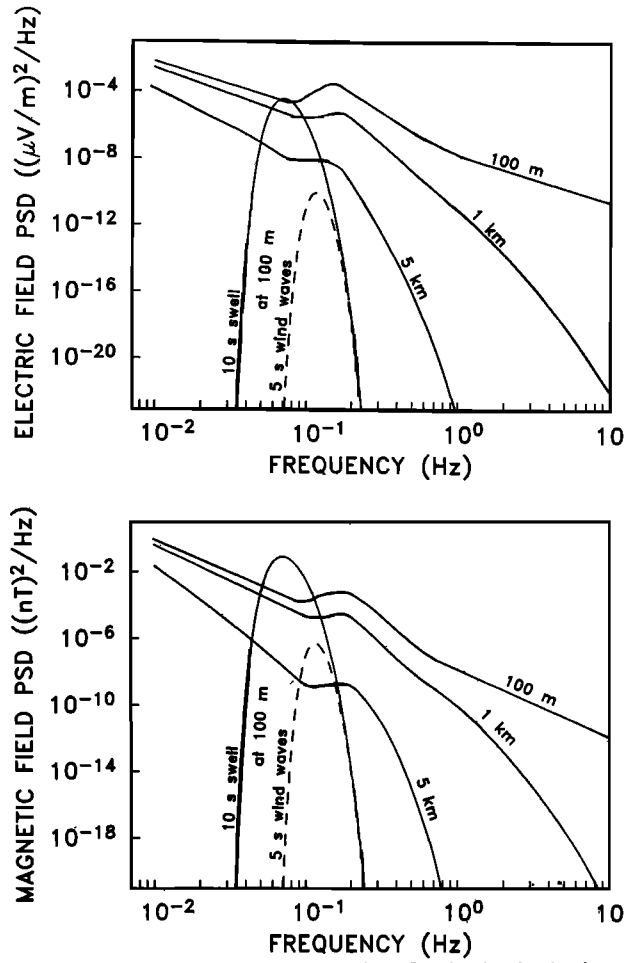

Fig. 12. The power spectral density of noise in the horizontal electric field (top) and the horizontal magnetic field (bottom) at the seafloor in water depths of 100 m, 1 km, and 5 km as a function of frequency from 0.01 to 10 Hz. The peaked functions centered near 0.1 and 0.2 Hz are the contributions from 10 s swell (solid) and 5 s wind waves (dashed) in 100 m of water; these terms vanish in deeper water. The gently sloping lines are the attenuated ionospheric contribution with a broad peak, centered near 0.2 Hz, representing the microseism source.

The calculation of the maximum source-receiver range for a given frequency depends on the conductivity-depth relation. At 1 Hz with a lithospheric conductivity of 0.05 S/m in 1 km of water and using a 6×10^4 A m source a signal level comparable to the noise level is achieved at a range of 15 km using a receiver with a 10-m antenna and a bandwidth of 10^{-4} Hz. Smaller bandwidths can be achieved by increasing signal integration time, raising the maximum range. In practice, instrumental electronic noise and attenuation of the fields by highly conductive sediments will probably be the limiting factor. Since the lithospheric conductivity is probably much lower than 0.05 S/m, longer ranges can be attained. If integration times of 1 week are used, ranges in excess of 50 km can be attained. The maximum horizontal range reflects the vertical region that is sampled by the electromagnetic fields; hence measurement of the lithospheric conductivity to considerable depths is feasible.

APPENDIX A: ELECTROMAGNETIC FIELDS FOR A FINITE HED IN SHALLOW WATER

The expressions (22) and (23) are valid when reflections off of the thermocline and sea surface are not important and for source-receiver distances much larger than the length of the source wire. Inclusion of upper conductive structure requires an additional pair of response functions evaluated at the upper boundary ($z = H$) given by

$$\lambda = -\left.\frac{\Psi}{\partial_z \Psi}\right|_{z=H} \tag{A1}$$

$$\kappa = \left.\frac{-\sigma\Pi}{\partial_z \Pi}\right|_{z=H} \tag{A2}$$

and reflection coefficients given by (25) and (26) with (A1) and (A2) substituted for (20) and (21). We consider a finite wire of length dl oriented along the x' axis with azimuth ϕ'. Replacing p in (23) and (24) with Idx', where I is the source current, yields

$$\Psi(\rho,z,\omega) = -\frac{\mu I}{4\pi}\,\partial_y \int_{-L}^{L} dx' \int_0^\infty dk\, J_0(k\zeta)\,\frac{1}{k\beta_0} \left[\frac{R_{TE}^{\downarrow}}{Z} e^{-\beta_0(z+z')} + \frac{R_{TE}^{\uparrow}}{Z} e^{-2\beta_0 H} e^{\beta_0(z+z')} + \frac{\Gamma}{Z}\right] \tag{A3}$$

$$\Pi_h(\rho,z,\omega) = \frac{\mu I}{4\pi}\,\partial_x \int_{-L}^{L} dx' \int_0^\infty dk\, J_0(k\zeta)\,\frac{1}{k} \left[\frac{R_{TM}^{\downarrow}}{\Delta} e^{-\beta_0(z+z')} - \frac{R_{TM}^{\uparrow}}{\Delta} e^{-2\beta_0 H} e^{\beta_0(z+z')} \mp \frac{E}{\Delta}\right] \tag{A4}$$

where

$$\Gamma = e^{-\beta_0|z-z'|} + R_{TE}^{\uparrow}\, R_{TE}^{\downarrow}\, e^{-2\beta_0 H}\, e^{\beta_0|z-z'|} \tag{A5}$$

$$Z = 1 - R_{TE}^{\uparrow}\, R_{TE}^{\downarrow}\, e^{-2\beta_0 H} \tag{A6}$$

$$E = e^{-\beta_0|z-z'|} - R_{TM}^{\uparrow}\, R_{TM}^{\downarrow}\, e^{-2\beta_0 H}\, e^{\beta_0|z-z'|} \tag{A7}$$

$$\Delta = 1 - R_{TM}^{\uparrow}\, R_{TM}^{\downarrow}\, e^{-2\beta_0 H} \tag{A8}$$

and ζ is given by (19). The denominators (A6)–(A8) may be expanded into a power series, and the result represents an infinite number of reflections in the waveguide between seafloor and sea surface. Application of (5) and (11) to (A3) and (A4) is straightforward but tedious and will be omitted. Since ζ is dependent on both ρ and ϕ, the derivatives of $J_0(k\zeta)$ contain terms like

$$\partial_\rho \zeta = \left[\frac{\rho - \rho'\cos(\phi-\phi')}{\zeta}\right] \tag{A9}$$

$$\frac{1}{\rho}\,\partial_\phi \zeta = \frac{\rho'\sin(\phi-\phi')}{\zeta} \tag{A10}$$

$$\partial_x \zeta = \left[\frac{\rho\cos\phi - \rho'\cos\phi'}{\zeta}\right] \tag{A11}$$

$$\partial_y \zeta = \left[\frac{\rho\sin\phi - \rho'\sin\phi'}{\zeta}\right] \tag{A12}$$

Calculation of the finite HED fields is accomplished by quadrature, with an integrand consisting of successive evaluations of the electromagnetic fields for different source points.

APPENDIX B: ANALYTIC EVALUATION OF THE SOURCE TERMS

In each of (27)–(35) the source terms corresponding to the rapidly damped direct wave in the ocean can be expressed analytically, using the results of *Watson* [1962] and the derivative relationships for Bessel functions. The integrals are

$$\int_0^\infty dk\, J_1(k\rho) k^2 e^{-\beta_0|z-z'|} = \frac{|z-z'|\rho e^{-\gamma_0 R}}{R^5}(\gamma_0^2 R^2 + 3\gamma_0 R + 3) \tag{B1}$$

$$\int_0^\infty dk\, J_1(k\rho)\,\frac{k^3}{\beta_0} e^{-\beta_0|z-z'|} = \frac{-\gamma_0 e^{-\gamma_0 R}}{R^4}(\gamma_0 R\rho^2 + 3\rho^2 - 2R^2) \tag{B2}$$

$$\int_0^\infty dk\, J_1(k\rho)\,\frac{k^2}{\beta_0} e^{-\beta_0|z-z'|} = \frac{\rho e^{-\gamma_0 R}}{R^3}(\gamma_0 R + 1) \tag{B3}$$

$$\int_0^\infty dk\, J_0(k\rho) k\beta_0 e^{-\beta_0|z-z'|} = \frac{e^{-\gamma_0 R}}{R^5}\{\gamma_0^2 R^2 (z-z')^2 + (\gamma_0 R+1)[2(z-z')^2 - \rho^2]\} \tag{B4}$$

$$\int_0^\infty dk\, J_0(k\rho)\,\frac{k}{\beta_0} e^{-\beta_0|z-z'|} = \frac{e^{-\gamma_0 R}}{R} \tag{B5}$$

$$\int_0^\infty dk\, J_0(k\rho) k e^{-\beta_0|z-z'|} = \frac{|z-z'|e^{-\gamma_0 R}}{R^3}(\gamma_0 R + 1) \tag{B6}$$

where

$$R = \sqrt{\rho^2 + (z-z')^2}$$

and $\gamma_0 = \sqrt{i\omega\mu\sigma_o}$. Each of (B1)–(B6) effectively vanishes within a few skin depths of the source due to the exponential term.

APPENDIX C: AVERAGING WELL LOG CONDUCTIVITY VALUES

Electrical conductivity logs from DSDP boreholes display a wide scatter from point to point, reflecting the inhomogeneous nature of the basalts as well as the effect of drilling disturbance. For interpretation purposes it is necessary to average the data, but this should be done in a manner consistent with the physical mechanism governing the conduction process. At low temperatures in the pres-

ence of conducting fluids like seawater the electrical conductivity often follows Archie's law [*Shankland and Waff*, 1974].

$$\sigma = \sigma_w p^n \tag{C1}$$

where σ_w is the electrical conductivity of the fluid and p is the mean porosity. The exponent n is estimated to lie close to 2. For the ith measurement in a well the effective porosity p_i is given by rearranging (C1)

$$p_i = (\sigma_i/\sigma_w)^{1/n} . \tag{C2}$$

Combining N measurements of conductivity by averaging (C2) yields the mean porosity for the section. Combining this with (C1) yields

$$\bar{\sigma} = (\sigma_w)^{[(n-1)/n]} \overline{\sigma^{1/n}} \tag{C3}$$

as a mean value for the formation electrical conductivity. For $n = 2$ the mean conductivity is the geometric mean of the square roots of the fluid and formation average conductivity from (C2). This brings well log results into agreement with results from the large-scale resistivity experiment.

Acknowledgments. R. L. Parker provided many useful discussions about numerical methods. This work was supported by the Earth Physics branch of the Office of Naval Research and the Scripps Industrial Associates.

REFERENCES

Anderson, W. L., Numerical integration of related Hankel transforms of orders 0 and 1 by adaptive digital filtering, *Geophysics, 44*, 1287–1305, 1979.

Chave, A. D., Lithospheric structure of the Walvis Ridge from Rayleigh wave dispersion, *J. Geophys. Res., 84*, 6840–6848, 1979.

Chave, A. D., On the theory of electromagnetic induction in the earth by ocean currents, submitted to *Geophys. J. R. Astron. Soc.*, 1982.

Chave, A. D., R. P. von Herzen, K. A. Poehls, and C. S. Cox, Electromagnetic induction fields in the deep ocean northeast of Hawaii: Implications for mantle conductivity and source fields, *Geophys. J. R. Astron. Soc., 66*, 379–406, 1981.

Coleman, R. G., Tectonic setting for ophiolite obduction in Oman, *J. Geophys. Res., 86*, 2497–2508, 1981.

Cox, C. S., Electromagnetic induction in the oceans and inferences on the constitution of the earth, *Geophys. Surv., 4*, 137–156, 1980.

Cox, C. S., On the electrical conductivity of the oceanic lithosphere, *Phys. Earth Planet. Inter., 25*, 196–201, 1981.

Cox, C. S., J. H. Filloux, and J. C. Larsen, Electromagnetic studies of ocean currents and electrical conductivity below the ocean floor, in *The Sea*, vol. 4, part 2, edited by A. E. Maxwell, pp. 637–693, Interscience, New York, 1970.

Cox, C. S., N. Kroll, P. Pistek, and K. Watson, Electromagnetic fluctuations induced by wind waves on the deep-sea floor, *J. Geophys. Res., 83*, 431–442, 1978.

Cox, C. S., T. K. Deaton, and P. Pistek, An active source EM method for the seafloor, submitted to *Radio Sci.*, 1981.

Edwards, R. N., L. K. Law, and J. M. DeLaurier, On measuring the electrical conductivity of the ocean crust by a modified magnetometric resistivity method, *J. Geophys. Res., 86*, 11609–11615, 1981.

Filloux, J. H., Magnetotelluric soundings over NE Pacific may reveal spatial dependence of depth and conductance of the asthenosphere, *Earth Planet. Sci. Lett., 46*, 244–252, 1980.

Filloux, J. H., Magnetotelluric exploration of the North Pacific: Progress report and preliminary soundings near a spreading ridge, *Phys. Earth Planet. Inter., 25*, 187–195, 1981.

Gregory, R. T., and M. P. Taylor, An oxygen isotope profile in a section of Cretaceous ocean crust, Samail ophiolite, Oman: Evidence for $\delta^{18}O$ buffering of the oceans by deep (>5 km) seawater-hydrothermal circulation at mid-ocean ridges, *J. Geophys. Res., 86*, 2737–2755, 1981.

Horne, R. A., and C. R. Frysinger, The effect of pressure on the electrical conductivity of sea water, *J. Geophys. Res., 68*, 1967–1973, 1963.

Keller, G. V., Electrical prospecting for oil, *Q. Colo. Sch. Mines, 63*, 1–268, 1968.

Larsen, J. C., The electromagnetic field of long and intermediate water waves, *J. Mar. Res., 29*, 28–45, 1971.

Law, L. K., and J. H. Greenhouse, Geomagnetic variation sounding of the asthenosphere beneath the Juan de Fuca Ridge, *J. Geophys. Res., 86*, 967–978, 1981.

Morse, P. M., and H. Feshbach, *Methods of Theoretical Physics*, 1978 pp., McGraw Hill, New York, 1953.

Pallister, J. S., and C. A. Hopson, Samail ophiolite plutonic suite: Field relations, phase variation, cryptic variation and layering, and a model of a spreading ridge magma chamber, *J. Geophys. Res., 86*, 2593–2644, 1981.

Patterson, T. N. L., Algorithm for automatic numerical integration over a finite interval, *Commun. A. C. M., 16*, 694–699, 1973.

Phillips, O. M., *The Dynamics of the Upper Ocean*, 2nd ed., 336 pp., Cambridge University Press, Cambridge, 1977.

Rai, C. S., and M. H. Manghnani, Electrical conductivity of basalts to 1550°C, Magma Generation, edited by H. J. B. Dick, *Bull. Oreg. Dep. Geol. Miner. Ind., 96*, 219–232, 1977.

Rai, C. S., and M. H. Manghnani, Electrical conductivity of ultramafic rocks to 1820 Kelvin, *Phys. Earth Planet. Inter., 17*, 6–13, 1978.

Ranganyaki, R. P., and T. R. Madden, Generalized thin sheet analysis in magnetotellurics: An extension of Price's analysis, *Geophys. J. R. Astron. Soc., 60*, 445–457, 1980.

Salisbury, J. H., and N. I. Christensen, The seismic velocity structure of a traverse through the Bay of Islands ophiolite complex, Newfoundland, an exposure of oceanic crust and upper mantle, *J. Geophys. Res., 83*, 805–817, 1978.

Shankland, T. J., Electrical conductivity in rocks and minerals: Parameters for interpretation, *Phys. Earth Planet. Inter., 10*, 205–219, 1975.

Shankland, T. J., and H. S. Waff, Conductivity in fluid-bearing rocks, *J. Geophys. Res., 79*, 4863–4868, 1974.

Souriau, A., The upper mantle beneath Ninetyeast Ridge and Broken Ridge, Indian Ocean, from surface waves, *Geophys. J. R. Astron. Soc., 67*, 359–374, 1981.

Stesky, R. M., and W. F. Brace, Electrical conductivity of serpentinized rocks to 6 kilobars, *J. Geophys. Res., 78*, 7614–7621, 1973.

von Herzen, R. P., T. J. G. Francis, and K. Becker, In-situ large scale electrical resistivity of ocean crust, site 504B, *Initial Rep. Deep Sea Drill. Proj., 69/70*, in press, 1981.

Wait, J. R., The electromagnetic fields of a horizontal dipole in the presence of a conducting half-space, *Can. J. Phys., 39*, 1017–1028, 1961.

Watson, G. N., *A Treatise on the Theory of Bessel Functions*, 2nd ed., 804 pp., Cambridge University Press, Cambridge, 1962.

Webb, S., and C. S. Cox, Electromagnetic fields induced at the seafloor by Rayleigh-Stoneley waves, *J. Geophys. Res., 87*, 4093–4102, 1982.

Wertz, R., and W. H. Campbell, Integrated power spectra of geomagnetic field variations with periods of 0.3–300 s., *J. Geophys. Res., 81*, 5131–5140, 1976.

Young, P. D., and C. S. Cox, Electromagnetic active source sounding near the East Pacific Rise, *Geophys. Res. Lett., 8*, 1043–1046, 1981.

(Received December 9, 1981;
revised April 14, 1982;
accepted April 16, 1982.)